Five-Parameter Grain Boundary Inclination Recovery with EBSD and Interaction Volume Models

CAROLINE SORENSEN, JOHN A. BASINGER, MATTHEW M. NOWELL, and DAVID T. FULLWOOD

While electron backscatter diffraction (EBSD) patterns are often used to present two-dimensional information about a material microstructure, they are in fact a product of the three-dimensional electron interaction volume. Consequently, 3D spatial information exists in EBSD images, which is generally not accessed. Specifically, the inclination of the grain boundary plane may be observed in EBSD patterns taken near grain boundaries. If, at the same time, the shape of an electron interaction volume in the material is known, a grain boundary plane normal direction can be obtained from a sequence of EBSD images taken stepwise in a line crossing the grain boundary. Here, these two principles are used for demonstrating the determination of grain boundary normal vectors from EBSD images. Coherent twin boundaries and focused ion beam serial scan data are used for validation. Results indicate a mean error for this approach of 3 deg with a standard deviation of 3.8 deg.

DOI: 10.1007/s11661-014-2345-7

I. INTRODUCTION

GRAIN boundaries have a significant effect on material properties. Depending on the interfacial energies of the boundaries, the presence of certain types of grain boundaries can either assist or degrade several material behaviors and properties (*e.g.*, creep, corrosion, precipitation of solute atoms, and electrical or thermal conductivity). This energy at the boundary is partially dependent on the grain boundary's inclination.[1] Electron backscatter diffraction (EBSD) has been useful in boundary characterization because of its ability to identify grain orientations and the misorientation angle between points on either side of a grain. Coincident site lattice (CSL) theory has been used extensively with EBSD scans to identify grain boundary types with favorably low interface energies without knowledge of the grain boundary plane inclination.[2–4] However, the true coherence and beneficial nature of such boundaries is also significantly influenced by the grain boundary plane normal.[5]

In order to also recover the full five-parameter grain boundary character[6] of a material (three variables for a grain orientation, and two for the grain boundary plane normal) using EBSD, one currently must use focused ion beam (FIB), manual serial sectioning, or stereology[7] to reconstruct the full 3D grain boundary character. Unfortunately, these techniques are destructive to the material and prohibit in situ experiments.

Synchrotron-based X-ray diffraction and imaging techniques can access orientation as well as 3D grain shape non-destructively for a recovery of the full grain boundary character.[8] The spatial resolution of this approach is limited to the micrometer scale (*vs* tens of nanometers in EBSD). Here, a technique is presented for the non-destructive determination of grain boundary plane normals (and orientations) using the saved EBSD images from a single OIM scan.

EBSD images result from the diffraction of electrons that are scattered out of the sample from within a 3D volume, called the electron interaction volume. Information regarding the crystal structure that is extracted from these images (such as orientation) is typically treated as 2D data.

In the case where the interaction volume contains more than one lattice configuration, the indexing software (in this case, OIM™) decodes only the structure with the stronger pattern. The other structure's information is discarded in the indexing process. However, if the envelope of the interaction volume is known, and the relative strength of each pattern within a single image can be determined, information regarding the geometry of the boundary between the two structure types can be determined.

This paper will demonstrate a framework for extraction of grain boundary character (more particularly, grain boundary inclination) through the application of the following steps:

(1) Model the envelope of the interaction volume
(2) Create a library of simulated curves representing the convolution of the interaction volume and with a range of grain boundary angles.

CAROLINE SORENSEN, Undergraduate Student, formerly with the Department of Mechanical Engineering, Brigham Young University, Provo, UT, is now with MIT, Cambridge, MA. JOHN A. BASINGER, PhD Student, formerly with the Department of Mechanical Engineering, Brigham Young University, is now with Southwest Research Institute, San Antonio, TX. MATTHEW M. NOWELL, Senior Scientist, is with the TSL-EDAX/AMETEK, Draper, UT. DAVID FULLWOOD, Associate Professor, is with the Department of Mechanical Engineering, Brigham Young University. Contact e-mail: dfullwood@byu.edu
Manuscript submitted May 29, 2012.
Article published online June 11, 2014

(3) Determine the relative strength of mixed EBSD patterns across a boundary (characteristic curve).
(4) Recover grain boundary inclination by comparison of curve library and the characteristic curve.

Note that Chen and Kuo[9] recently produced similar curves to the ones presented in this paper, although not for the analysis of grain boundary angle determination; the paper by Chen was also published after the initial submission of the current paper.

II. BACKGROUND

The interaction volume of an EBSD image is the volume within the sample from which the electrons that impact the phosphor screen are ejected. The size, shape, and electron density of this region are dependent on a myriad of factors including both intrinsic parameters (*e.g.*, the material composition and density) and extrinsic parameters (*e.g.*, the sample tilt, initial accelerating voltage, and diameter of the incident electron beam).[10] Because Monte Carlo methods lend themselves well to the issue of interaction volume modeling, various programs exist to simulate this phenomenon.[11–13]

If the incident electron beam is sufficiently close to a grain boundary, the EBSD image will reflect the crystallography of both grains at once. This results in mixed EBSD patterns, which can be separated into dimmed versions of the parent images using cross-correlation with reference images (*i.e.*, images containing patterns exclusively from either grain).[14] The level of this pattern mixing is dependent on the proportion of the interaction volume in either grain, which is, in turn, dependent on the orientation of the grain boundary plane.

The method will be validated using serial OIM scan data (recording all EBSD images in each layer) of copper and twin boundaries in tantalum.

Validation of the above approach is done using 3D OIM data in copper and twin boundaries in tantalum. The inclination of the grain boundary plane can be found using a FIB for serial section scanning. The FIB allows for the incremental removal of thin layers of the sample between scans. From these slices of a material, the full orientation of the grain boundary can be found, at the expense of destroying the sample.

For twin boundaries, the angle of the grain boundary plane below the surface can be calculated based on the geometry of the parent grain. This exploits the fact that twins form on specific planes for a given crystal structure (*e.g.*, {111} for face-centered cubic (FCC) and {112} for body-centered cubic (BCC) crystals).

III. METHOD

We specify the reference frame from which the grain boundary normals are to be measured as shown in Figure 1. This reference coordinate system, also referred to as the "sample frame," was chosen consistent with the OIM™ scan map display.

A grain boundary orientation is defined by the two angles that characterize its normal: θ, the angle between the positive x-axis and the projection in x–y plane, and φ, the angle from the x–y plane, moving toward the positive z-axis (Figure 2).

Determining the grain boundary orientation is essentially a four step process. First, a Monte Carlo simulation is run specific to the material being used. Second, a library of possible characteristic curves specific to the grain boundary inclination is created. Third, a pattern strength curve is calculated from the relative strength of patterns crossing a grain boundary in a line using experimental EBSD patterns. Fourth, the slope of the experimental curve is extracted and the best match between the experimental curve and library curves is used to identify the grain boundary plane character. Note that the individual EBSD images must be saved at each scan point.

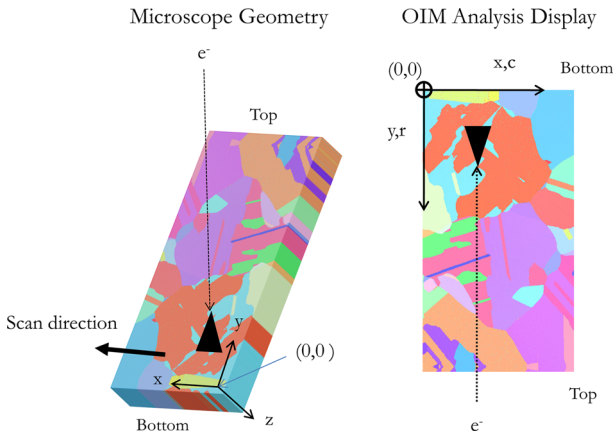

Fig. 1—Reference coordinate frame and electron interaction volume (shown as a black triangle at the point where the electron beam intersects the surface) (color figure online).

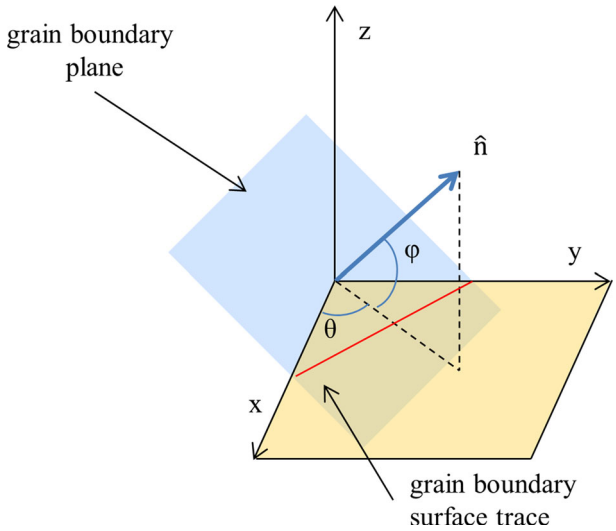

Fig. 2—Grain boundary normal angles, φ and θ. The grain boundary plane is shown protruding from the sample surface plane. The normal to the grain is labeled $\hat{\mathbf{n}}$ (color figure online).

A. *Step 1: Monte Carlo Simulation*

Monte Carlo simulations are useful for modeling electron interaction volumes because of the variation in energy loss and electron trajectory that occur in the electron/atom collisions. Each individual electron trajectory is calculated as a series of collision and scattering events. While the resultant set of trajectories does not contain information regarding the sophisticated electron and lattice interactions that result in the EBSD patterns, it does provide vital information regarding interaction depth and resultant electron energy. This approach has been used in various environments, including in connection with EBSD.[9,15–18] In this work, 20,000 trajectories were calculated using MATLAB code based on Monte Carlo algorithms from Joy's book.[11] This number of trajectories was chosen to provide a significant margin above the successful work of Ren *et al.*,[19] who used 10,000 trajectories. In order to only capture electrons of sufficient energy to contribute to a backscatter diffraction pattern,[10] initial and cutoff accelerating voltages of 20 and 19 keV, respectively, were used. Only a fraction of electrons backscatter out from the material's surface. As previously mentioned, the backscattered fraction of the total incident electrons is dependent on both material properties and microscope settings. The materials used were copper and tantalum. The microscope settings for both materials were 20 keV accelerating voltage, 10 nm beam diameter, and 70 deg incident angle. The location of the last-scattering event before the electron exits the sample is recorded. These locations determine to which grain's pattern they contribute if the interaction pattern spans a grain boundary. Figure 3 shows the locations of these last-scattering events for backscattered electrons (BSEs) in a Monte Carlo simulation of tantalum.

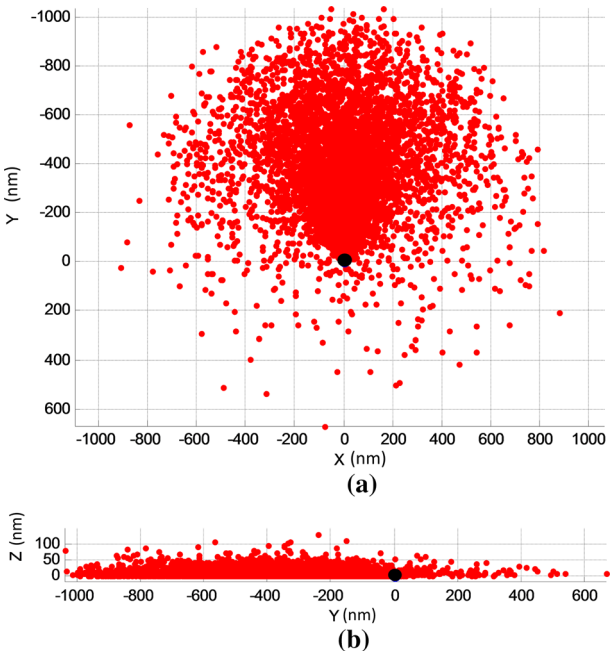

Fig. 3—Tantalum interaction volume, shown in the *X*–*Y*, and *Y*–*Z* planes, indicating the locations of the last BSE collisions. The positive z direction in the sample reference frame points into the material.

B. *Step 2: Creating a Library of Grain Boundary Curves*

The modeled interaction volume is divided by placing a theoretical grain boundary at some point on the *y*-axis (Figure 4). The ratio of BSEs contributing from one crystal (one side of the grain boundary) to the number of total BSEs is found. This grain boundary is then stepped through the simulated interaction volume, at intervals along the *y*-axis, identifying the ratio of BSEs on one side of the boundary at each location. This process simulates a line scan across a grain boundary. From this data, a curve is plotted that shows the contribution of one crystal at a sequence of locations across the grain boundary (Figure 5). This curve will be referred to as the "characteristic curve." This procedure of finding characteristic curves is repeated for each potential grain boundary inclination (using 2 deg steps in θ and φ). The angles θ and φ of the simulated grain boundary plane normal ranged from 0 to 180 deg and −90 to 90 deg, respectively. Together, the set of curves characterizing all possible grain boundary orientations forms a curve library for the material and microscope settings used in that particular Monte Carlo simulation. The library of curves is also specific to the *y*-axis and used for comparison only with series of actual mixed EBSD images in the y direction.

For this work, curve libraries were made of all possible simulated grain boundary planes for copper and tantalum. These two materials were tested for to their ease of validation using existing samples. An

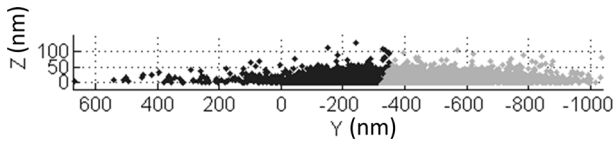

Fig. 4—Last backscatter electron collisions shown for an interaction volume divided by a grain boundary plane. The positive z direction in the sample reference frame points into the material.

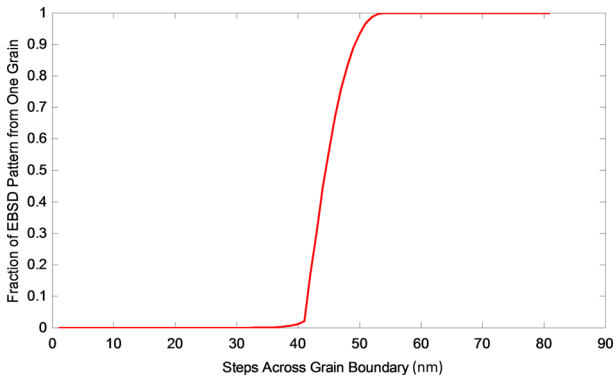

Fig. 5—Fraction of the interaction volume on one side of a simulated grain boundary (located at 45 nm in this schematic), for a beam moving along the *y*-axis.

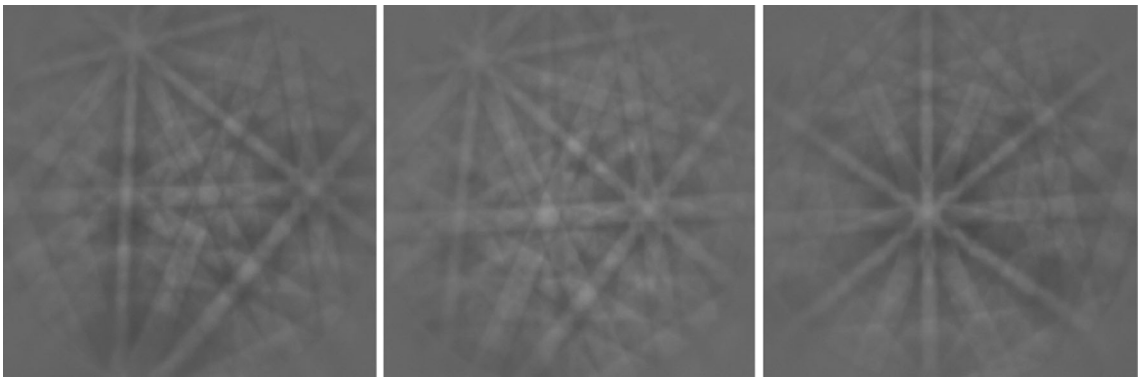

Fig. 6—Mixed EBSD pattern (middle) with contributing patterns on either side.

interaction volume size was determined by taking the envelope of all final scattering events for electrons with a final energy above 95 pct of their original energy (*i.e.*, the volume from which electrons assumed to contribute to the EBSD pattern escaped). Using this approach, the calculated interaction volume size for copper was in agreement with published values.[19] Analogous data for tantalum were not available.

C. *Step 3: Experimental Grain Boundary Curve*

The following is a description of the process used to identify real characteristic curves in an EBSD scan. The cross-correlation separation is based on work done by Kacher *et al.*[14]:

3.1 Unmixed reference patterns are selected using either method (a) or (b).

- (a) Two reference patterns are selected from within each grain on either side of a boundary away from any grain boundaries.
- (b) Where unmixed reference patterns are not available simulated patterns may be used to extract reference images from mixed patterns (described below).

3.2 A sequence of images taken from points along a line in the negative y direction that cross the grain boundary is selected. Many of the images in the sequence will contain mixed EBSD patterns (Figure 6 shows an example of a mixed EBSD image in nickel).

3.3 All images are band-pass filtered to remove low frequency variations in intensity and high frequency noise. This removes noise and allows for a smooth average background.

3.4 Normalized cross-correlation comparison is done between the reference image from one grain and each mixed pattern in the line crossing the grain boundary.

3.5 The maximum value of the normalized cross-correlation of the reference image with each mixed image is recorded by location on the line crossing the boundary, which is along the y-axis.

3.6 Step 3.4 is repeated using the reference image from the second grain, generating two such curves for each sequence of images.

In this paper, the above process was applied to five nearby vertical line scans of images crossing the same boundary. This gave ten experimental curves for each distinct boundary. Curves whose maximum slope deviated from the mean slope of the ten curves by more than 1SD were discarded, and a new mean slope was calculated and used for comparison with the library of simulated curves' slopes.

D. *Step 4: Comparison Between the Simulated Library and Experimental Curve*

A real grain boundary curve, as obtained by normalized cross-correlation (Step 3.4) often contains noisy data. The overall curve shape is consistently sigmoidal. However, local noise tends to obscure determination of the overall curve slope. Therefore, some pre-processing is required before comparison with the simulated curve library slopes. The experimental curve is smoothed initially using local moving average filter with a span of five elements. In addition, the slopes of several points around the inflection point are averaged, to insure that the maximum slope measured is not altered by local roughness.

In addition to smoothing the pattern strength curve, the grain boundary trace angle as viewed on the sample surface is also determined. The surface trace angle is measured by taking the arc-tangent of the ratio of y and x distances of a line drawn over the grain boundary (distances determined in the OIM software). Adding 90 deg to the trace angle gives the grain boundary normal angle, θ, on the surface (x–y plane). If necessary, θ is adjusted by 180 deg to insure that it is always positive and less than or equal to 180 deg.

Finally, comparison is made between the maximum slope of the actual grain boundary convolution curve and the slope of each simulated boundary curve in the library. Using this simple approach does not lead to a one–one correspondence between curves and boundary character (expressed in terms of θ and φ). The slope of the curve relates to the rate at which one grain leaves the interaction volume and the other enters. Hence, a given slope can be achieved by various configurations of the

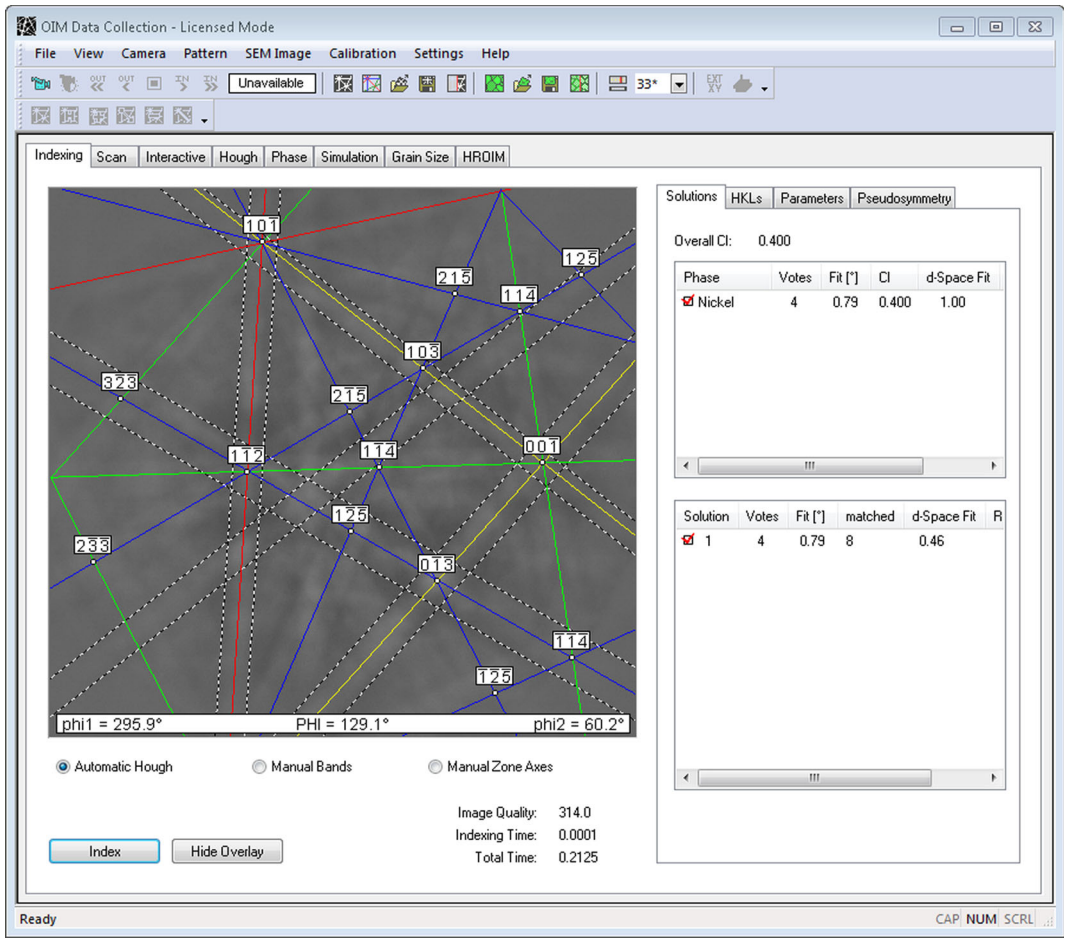

Fig. 7—Indexed mixed EBSD image in OIM DC software (color figure online).

trace and inclination angle. However, for a particular surface trace angle, θ, there is only one subsurface inclination angle, φ, whose characteristic curve fits the experimental one. Thus by knowing the surface trace angle in addition to the characteristic curve, the matching process becomes fully deterministic. By using this process, the best-matching slope is selected, identifying the grain boundary plane normal (expressed in θ and φ) at the location on the scan crossed by the line of EBSD images.

E. *Using Simulated Reference Patterns*

There exist cases where an unmixed pattern is not available for use as a reference pattern (when creating a pattern strength curve across a boundary). One such case occurs when grain sizes are on the order of the interaction volume size. In such a case, simulated EBSD patterns may be used in the separation of patterns for indexing.

An example of simulating reference patterns is given here starting from a mixed pattern in a nickel sample. The mixed nickel pattern is loaded into OIM Data Collection (OIM DC). The pattern is indexed, and the orientation, pattern center, and relevant microscope settings are recorded (Figure 7). Using MATLAB, a Bragg's law-based simulated pattern is then generated based on the recorded information[20] (Figure 8). This is used as the first reference EBSD image as its Kikuchi

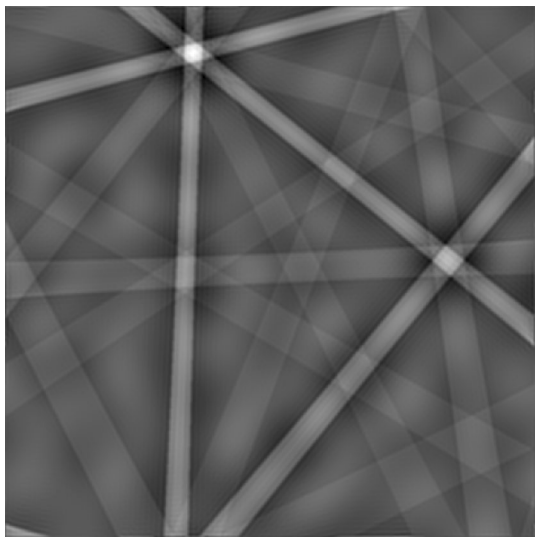

Fig. 8—Simulated image of the prominent orientation in the mixed nickel pattern.

bands correspond to one of the two orientations within the original image.

The prominent bands in the simulated pattern are identified and all pixels belonging to the bands are a new intensity value of 1. All other background intensities are given the value 0, creating a black and white image. This image is then weighted to give the bands an intensity consistent with the average intensity of the mixed nickel pattern.

Next, this intensity-weighted pattern is subtracted from the original mixed-intensity EBSD image. The resulting image is saved and loaded again into OIM DC to be indexed. Identification of the second pattern in the OIM software indicates the second crystal orientation (Figure 9), which may then be used (all other parameters being the same) to simulate a second reference pattern. The pair of unmixed simulated reference images may then be used in place of actual unmixed EBSD images.

F. *Validation of the Grain Boundary Inclination Recovery*

To test the presented approach for finding the grain boundary orientation, the results were initially validated using a three-dimensional dataset of copper. The data were compounded from serial EBSD scans using the FIB to remove a layer of material between scans. A second verification used twin grain boundaries in tantalum.

For the serial scan data, the FIB beam removed 500 nm of material between each of the 20 OIM surface scans taken. The scans were then registered spatially by the software. The scan dimensions were 49 μm by 20 μm with a 0.2 μm step size. Due to the small area viewed, only a few grain boundaries were well characterized within the volume.

For the twin boundary verification, the grain orientation and the surface trace of the grain boundary constrain the possible values of the grain boundary normal vector component φ (through the thickness of the material) to only a few options (depending on crystal symmetry, as mentioned in Section I).

In tantalum, which possesses BCC crystal symmetry, twin planes occur on the {112} family of planes. All possible plane normal directions for cubic symmetry were calculated and then rotated into the crystal frame based on the Euler angles of the parent grain. The rotated plane normals for each possible plane were projected onto the x–y plane and compared with the measured twin grain boundary normal's θ component on the scan surface. The smallest angle between the

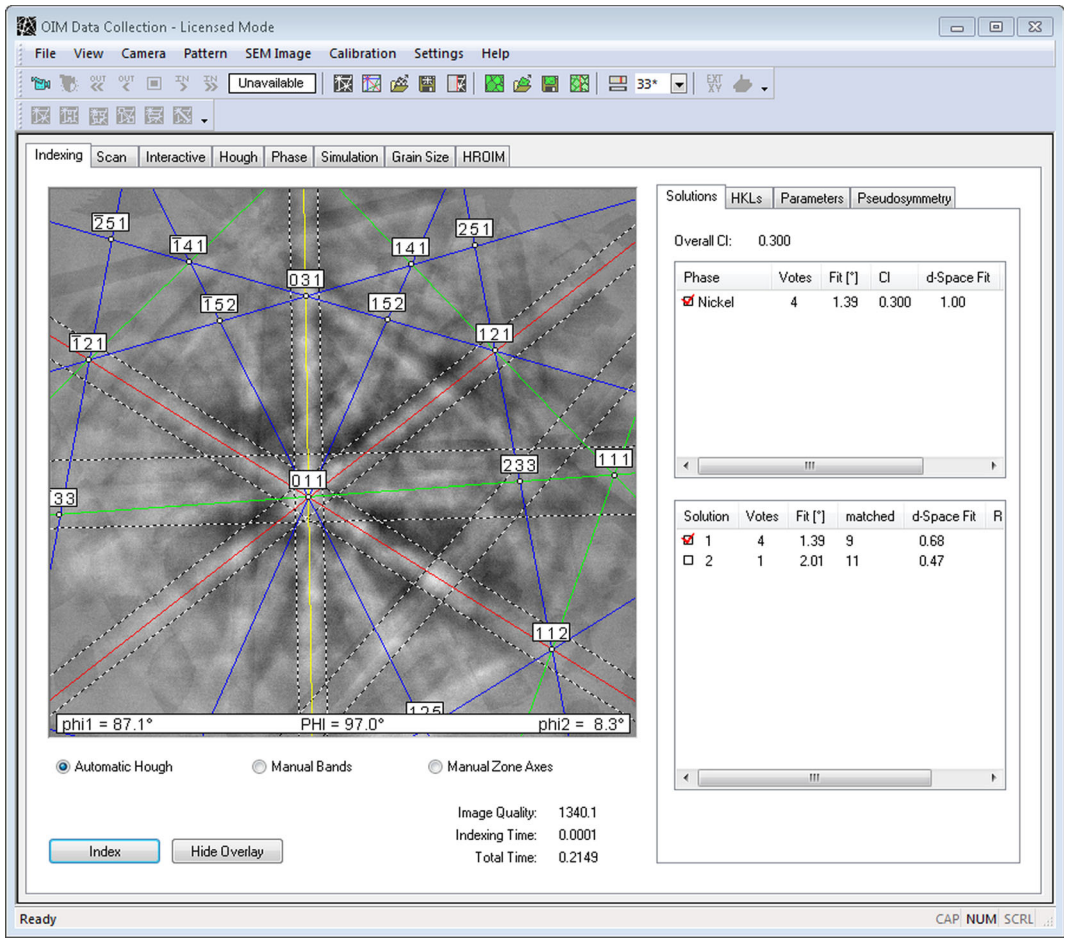

Fig. 9—Indexing of mixed EBSD image with bands simulated from the stronger orientation removed (color figure online).

normal projections and the surface trace normal identifies the best candidate and hence the φ angle.

IV. RESULTS

The use of characteristic curve libraries to determine subsurface grain boundary plane orientation proved successful, with a maximum error of 11 deg and an average error of 3 deg. Fewer grain boundaries were accessible for validation in the copper data; therefore most of the results given are based on the tantalum twin boundaries.

A. *Copper Boundary*

Figure 10 shows the 3D composite of OIM scans from the copper sample. The angle φ was found using the shift in location of the boundary on the surface between layers 4 and 5 and the 500 nm separation between layers in the z direction. θ was measured from scan layer 4. The angles θ and φ were measured to be 46 and 63 deg, respectively, from the gathered FIB data.

Application of the new described methodology for determining φ predicted an angle of 66 deg, resulting in an error of 3 deg.

As described previously, twin boundaries provide constrained sets of possible boundary planes—assuming the orientation of both grains and the boundary's trace

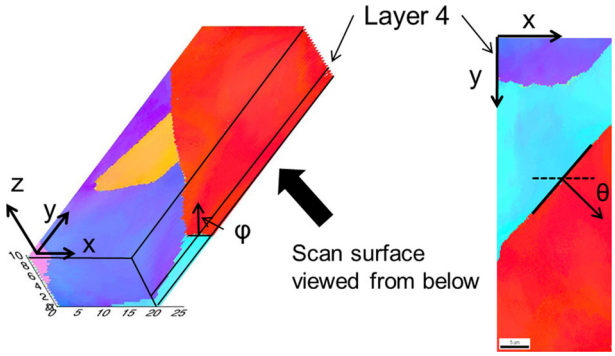

Fig. 10—Copper data from FIB serial scans. Grain boundary plane normal angles in φ and θ for scan (layer) four are determined to be $\theta = 46$ deg and $\varphi = 63$ deg, based on 500 nm spacing between layers. These experimentally determined angles are used for validation. Units for the labeled axes are in μm (color figure online).

angle are known. In this paper, twin boundaries found in multiple tantalum scans (from different areas on a single polished surface) were used for validating the grain boundary normal recovery method. Each scan contained numerous twin boundaries. Use of twins for validation did not require the destruction of the sample, as did the gathering of the FIB data.

Table I indicates the recovered grain boundary normal angle φ, given the measured θ angle of the twin boundary on the sample surface. It compares this φ angle to the φ angle required by the geometry of the twin boundary in tantalum.

Applying the simulated interaction volume method for determination of the full grain boundary normal to these given boundaries resulted in a mean error of 3 deg with a standard deviation of 3.8 deg.

V. DISCUSSION

A method for full determination of grain boundary plane normal directions is presented. This approach relies on the convolution of simulated grain boundaries and a simulated interaction volume for comparison with experimentally recovered characteristic curves crossing real grain boundaries. A Monte Carlo-based model of the electron interaction volume is used in conjunction with a single surface scan. The technique was validated using both a 3D copper serial scan and coherent twin boundaries from tantalum scans. The average error of this approach was found to be 3 deg, with a standard deviation of 3.8 deg. Although this statistical evaluation of the results is not particularly strong given that only seven tests were performed, the results are generally fairly close, with only one obvious outlier. Hence, we believe that the results are sufficient to be considered proof of concept for the method.

In this section, we discuss the sources of error currently present in the grain boundary inclination recovery method as well as challenges in any potential automation of this technique for consideration in future work.

Errors in the proposed method of recovery of grain boundary normal angles come from error introduced in the Monte Carlo simulation process and from error in the validation schemes. Within the simulation processes, there are several sources of inaccuracy. First, there is a discrepancy between the idealized settings used in the

Table I. The Predicted φ Angle from the Convolution Curve Comparison and the Error Between φ's is Given

Boundary	Measured θ	Twin φ	Predicted φ	Error
1	157.45	30.5828	30	0.5828
2	148.611	−47.5	−52	4.5
3	31.7783	54.7455	54	0.7455
4	112.271	−49.5114	−52	2.4886
5	66.7566	26.2763	26	0.2763
6	26.428	28.7793	26	2.77929
7	27.4177	35.3	24	11.3

All units are given in degrees.

Monte Carlo simulation and the exact conditions present in the microscope. For example, beam diameter is determined by a beam aperture setting in the microscope, which only gives an approximation of the beam diameter. Analogous errors may arise when specifying the incident angle, probe current, and density variation in the material from alloying. These errors are introduced regardless of the choice of any particular Monte Carlo simulation approach.

Furthermore, a cutoff is applied to electron energies escaping the surface. Electrons with energy less than the cutoff amount are not counted. In this paper, this cutoff value was chosen in accordance with what is generally believed to be minimum energy required for electrons to contribute to EBSD patterns (*i.e.*, 95 pct of their initial energy).[10] However, the simulated interaction volume size varies significantly based on the energy cutoff chosen, so this general rule of thumb may introduce some error into the interaction volume model. An additional way to improve the Monte Carlo model used here is to limit the recording of last-scattering events to only those electrons on a trajectory to intercept the phosphor screen.

The second source of error exists in the validation using the twin and FIB measurements. With the copper FIB data, the amount of material removed between layers is subject to variation. Any local changes in this thickness will influence estimates of the φ angle. For twin boundaries, errors in measurement of crystal orientation and surface trace angle will proportionately alter the indicated angle φ from the true angle. Measurement of θ is done by hand in the OIM software and is therefore also subject to small inaccuracies.

Lattice rotation close to the grain boundary may affect the shape of the curves. While this did not appear to be an issue for the materials tested in this paper, it might be an issue for highly deformed materials. We also note that the potential sharing of certain bands for patterns on either side of a twin may reduce the accuracy of the results; if bands are shared, the convolution method will find it harder to distinguish between the two patterns. In particular, this may help account for the larger error for certain of the twin boundary tests in Table I.

This work is presented as a proof of concept. While it has proved successful in initial testing, an automation of this grain boundary normal recovery technique presents some additional challenges yet to be addressed. One challenge to be noted in particular is that of several-patterns mixing near grain boundary triple junctions. Other challenges are presented in the cases of small grains, where an unmixed reference pattern does not exist, or over-large EBSD scan step sizes, where sufficient data about the change of mixing across a boundary are unavailable.

Among several other potential applications, this approach could prove useful, in conjunction with stereology, in the recovery 3D information of grain boundary character in statistically representative volume elements.

ACKNOWLEDGMENTS

The authors wish to acknowledge funding provided by the Army Research Office (WF911NF-08-1-0350) under Dr. David Stepp, Program Director. Caroline Sorensen was funded by REU supplements to NSF grants CMMI-0928923 and 1235365.

REFERENCES

1. A.P. Sutton and R.W. Balluffi: *Interfaces in Crystalline Materials*, Oxford University Press, Oxford, 1995.
2. T.Watanabe: in *Boundaries and Interfaces in Materials: The David A. Smith Symposium*, R.C. Pond, W.A.T. Clark, and A.H. King, eds., The Minerals, Metals and Materials Society, Warrendale, PA, 1998, pp. 19–29.
3. E.M. Lehockey, G. Palumbo, and P. Lin: in *Boundaries and Interfaces in Materials: The David A. Smith Symposium*, R.C. Pond, W.A.T. Clark, and A.H. King, eds., The Minerals, Metals and Materials Society, Warrendale, PA, 1998, pp. 45–50.
4. V. Randle: *Acta Metall. Mater.*, 1994, vol. 42, pp. 1769–84.
5. C.-S. Kim, A.D. Rollett, and G.S. Rohrer: *Scripta Mater.*, 2006, vol. 54, pp. 1005–09.
6. D.M. Saylor, A. Morawiec, and G.S. Rohrer: *Acta Mater.*, 2003, vol. 51, pp. 3663–74.
7. D.M. Saylor, B.S. El-Dasher, B.L. Adams, and G.S. Rohrer: *Metall. Mater. Trans. A*, 2004, vol. 35, pp. 1981–89.
8. A. King, M. Herbig, W. Ludwig, P. Reischig, E.M. Lauridsen T. Marrow, and J.Y. Buffière: *Nucl. Instrum. Methods Phys. Res. Sect. B*, 2010, vol. 268, pp. 291–96.
9. D. Chen and J.-C. Kuo: *Microsc. Microanal.*, 2013, vol. 19, pp. 4–7.
10. A. Deal, X. Tao, and A. Eades: *Surf. Interface Anal.*, 2005, vol. 37, pp. 1017–20.
11. D.C. Joy: *Monte Carlo Modeling for Electron Microscopy and Microanalysis*, Oxford University Press, New York, 1995.
12. D. Drouin, A.R. Couture, D. Joly, X. Tastet, V. Aimez R. Gauvin: *Scanning*, 2007, vol. 29, pp. 92–101.
13. N.W.M. Ritchie: DTSA-II. Gaithersburg, MD, 2011. http://www.cstl.nist.gov/div837/837.02/epq/dtsa2/index.html.
14. J. Kacher, B.L. Adams, D. Fullwood, C. Landon (2008) *In Applications of Texture Analysis,* John Wiley & Sons, Inc. 2008, pp. 147–54.
15. D.C. Joy: *Scanning Microsc.*, 1991, vol. 5, pp. 329–37.
16. W.S.M. Werner: *Surf. Interface Anal.*, 2001, vol. 31, pp. 141–76.
17. A. Deal, T. Hooghan, and A. Eades: *Ultramicroscopy*, 2008, vol. 108, pp. 116–25.
18. A. Winkelmann: *J. Microsc.*, 2010, vol. 239, pp. 32–45.
19. S.X. Ren, E.A. Kenik, K.B. Alexander, and A. Goyal: *Microsc. Microanal.*, 1998, vol. 4, pp. 15–22.
20. J. Kacher, C. Landon, B.L. Adams, and D. Fullwood: *Ultramicroscopy*, 2009, vol. 109, pp. 1148–56.